Hindawi Publishing Corporation
Journal of Nanomaterials
Volume 2014, Article ID 734751, 6 pages
http://dx.doi.org/10.1155/2014/734751

Research Article

Synthesis and Characterization of Silicon Nanoparticles Inserted into Graphene Sheets as High Performance Anode Material for Lithium Ion Batteries

Yong Chen, Xuejun Zhang, Yanhong Tian, and Xi Zhao

State Key Laboratory of Organic-Inorganic Composites, College of Materials Science and Engineering, Beijing University of Chemical Technology, Beijing 100029, China

Correspondence should be addressed to Xuejun Zhang; zhangxj@mail.buct.edu.cn

Received 29 May 2014; Accepted 24 July 2014; Published 19 August 2014

Academic Editor: Gaoshao Cao

Silicon nanoparticles have been successfully inserted into graphene sheets via a novel method combining freeze-drying and thermal reduction. The structure, electrochemical performance, and cycling stability of this anode material were characterized by SEM, X-ray diffraction (XRD), charge/discharge cycling, and cyclic voltammetry (CV). CV showed that the Si/graphene nanocomposite exhibits remarkably enhanced cycling performance and rate performance compared with bare Si nanoparticles for lithium ion batteries. XRD and SEM showed that silicon nanoparticles inserted into graphene sheets were homogeneous and had better layered structure than the bare silicon nanoparticles. Graphene sheets improved high rate discharge capacity and long cycle-life performance. The initial capacity of the Si nanoparticles/graphene keeps above 850 $mAhg^{-1}$ after 100 cycles at a rate of 100 mAg^{-1}. The excellent cycle performances are caused by the good structure of the composites, which ensured uniform electronic conducting sheet and intensified the cohesion force of binder and collector, respectively.

1. Introduction

During the past decade, secondary lithium ion batteries (LIBs) have become the major power source for mobile applications, such as cellular phones, digital cameras, and notebooks [1, 2]. Their rather high energy density of up to 120 $mAhg^{-1}$ makes LIBs superior to other battery types for mass market applications (e.g., lead-acid batteries: 30 $mAhg^{-1}$; nickel metal hydride batteries: 80 $mAhg^{-1}$) [3, 4].

State-of-the-art anodes of LIBs usually consist of graphite powder, in which lithium ions can be intercalated and deintercalated. Mechanical stability is provided by a polymeric binder, usually PVDF [5]. Besides graphite, which possesses a theoretical specific capacity of 372 $mAhg^{-1}$, there are several other promising materials for application as anode material in Li-ion batteries, with theoretical specific capacities superior to graphite, like tin [6, 7], SnO_2 [8], and Ge [9]. Unlike graphite, where lithium ions are stored in between the graphene layers in the graphite lattice during intercalation [10], silicon forms binary alloys with lithium [11–15]. Si nanowires having a structure of up to 500 nm in length is reported [16], resulting in a theoretical specific capacity of 4200 $mAhg^{-1}$.

Unfortunately, the alloying comes along with a significant volume change of around 300% [17], which leads to high mechanical stresses and, upon repeated cycling, to fast disintegration of the material and a very high irreversible capacity. In addition, the poor electrical conductivity of silicon (only 250 μSm^{-1}) leads to heat generation upon cycling due to the high internal resistance and limits the applicable charge current [18].

Intense research activities are currently undertaken in the field of carbon-silicon composites [6, 19, 20]. This group of materials seems to be a promising solution to overcome the silicon related problems discussed above. By using nanostructured silicon in the composites, mechanical stresses arising from volume changes will decrease, which leads to a reduced irreversible specific capacity. Such nanostructured materials can be prepared by, for example, ball-milling [21–23]. But, upon prolonged cycling, capacity fading due to loss of

electrical contact can still be detected. Superior performance could be expected if a good adhesion between the carbon and the nanostructured silicon would exist.

In this work, we designed Si nanoparticles/graphene multilayer structures by combining freeze-drying and thermal reduction. In this judiciously fabricated nanostructure, the flexible graphene films were designed to buffer the structural changes caused by volume expansion and contraction of Si layers during the Li alloying/dealloying processes. In addition, the graphene-film layers could isolate all Si nanoparticles, circumventing the Si aggregation problem. As a result, this facile approach can provide optimized graphene/Si nanoarchitectures where the graphene layers function as flexible mechanical support to mitigate and accommodate the volumetric-change-induced stresses/strains in the Si nanoparticles and therefore can alleviate or even avoid the pulverization of Si phase, maintaining the structural integrity of the electrodes at the same time. In addition, this reinforcing material offers an efficient, electrically conducting medium and effectively improves the adhesion strength between different active materials and also with Cu foil current collector [24]. Hence, these Si nanoparticles/graphene multilayer structure anodes exhibit a high reversible capacity and good capacity retention in both Li half cells and full cells.

2. Experimental

2.1. Materials Synthesis. The graphene was produced by modified Hummers' method. 4 mL of graphite oxide aqueous suspension (10.0 mg mL^{-1}) was diluted to 1.0 mg mL^{-1} with double distilled water and then sonicated for 60 min. Afterwards, 160 mg of silicon nanoparticles (<80 nm, Top Vendor Science & Technology Co., Ltd.) was dispersed in 20 mL of water via 40 min sonication (KQ3200DE, 40 kHz). Then, the achieved Si nanoparticles aqueous suspension was added to the above graphene oxide aqueous suspension, and the obtained mixture was sonicated for 30 min to obtain a uniform Si nanoparticles/graphene oxide aqueous suspension and then transferred into the freeze-drying apparatus with a temperature of −45°C. At this temperature, the pressure was slowly reduced and the frozen solvent was sublimated; then it was followed by reduction in a crucible in a tube furnace at 700°C for 2 h under H_2 (5 vol%)/Ar (95 vol%) atmosphere with a heating rate of 2°C min^{-1}, treatment with 20% HF water/ethanol solution, and drying under vacuum at 80°C to finally obtain Si nanoparticles/graphene composite.

2.2. Preparation of Test Cells. Negative electrodes slurry for 2025 type simulated cells was prepared by thoroughly mixing active material (85%) with carbon black (10%) and polytetrafluoroethylene (5%) in N-methylpyrrolidone (NMP). Electrodes with 0.5 cm^{-2} area and 0.02 mm depth extruding onto Cu foil were dried for 12 h at 120°C under vacuum. 2025 type coin cells were then assembled in an argon filled dry box using foils of Li metal as counter electrodes and Celgard 2400 as separators saturated with 1 M $LiPF_6$ in EC/EMC/DMC (1 : 1 : 1 in weight).

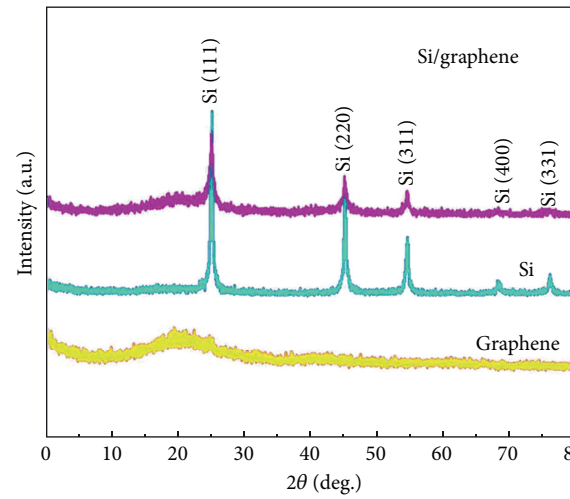

Figure 1: XRD patterns of the Si/graphene composites, Si nanoparticles, and graphene.

2.3. Morphology and Structure Tests. The surface morphology was observed by means of a scanning electron microscopy (SEM, TDCLS4800) and TEM (JEOL, JEM-2100). Powder X-ray diffraction (XRD) (Rigaku D/max-2400) was done to determine the material structure. Raman spectra were recorded on a Super LabRam-II spectrometer (JY-T6400) with a holographic grating of 1800 g mm^{-1}.

2.4. Electrochemical Tests. The cyclic voltammetry (CV) was performed by electrochemistry working station (Potentiostat/Galvanostat Model 263A). The constant current and constant voltage charge (CCCV charge) was performed by galvanostatic method.

3. Results and Discussion

3.1. Structural Properties and Morphology. Figure 1 shows the X-ray diffraction (XRD) patterns of the Si/graphene composites, Si nanoparticles, and graphene. The pattern of Si/graphene composites is the same as that of pure Si nanoparticles, implying that the silicon crystals in the Si/graphene composites are not destroyed during the freeze-drying and thermal reduction processes. For the Si nanoparticles/graphene, the major diffraction peaks are consistent with the pristine Si but exhibit a distinct decrease in peak intensity, revealing an entire encapsulation of Si by the graphene frame. In the XRD pattern of the graphene sample obtained with the same procedure of Si/graphene, the characteristic peak appears at 25.41, corresponding to a layer-to-layer distance (d-spacing) of 0.338 nm, which is close to the d-spacing of the natural graphite. The result confirms the well-packed layered structure of graphene. This characteristic peak is indistinctive in the pattern of Si/graphene, which might be attributed to the dispersion of graphene sheets by Si nanoparticles.

Figure 2 presents the Raman spectrum of the Si/graphene composites, with that of Si shown for comparison. For Si/graphene composites, a main peak at about 527 cm^{-1} is in

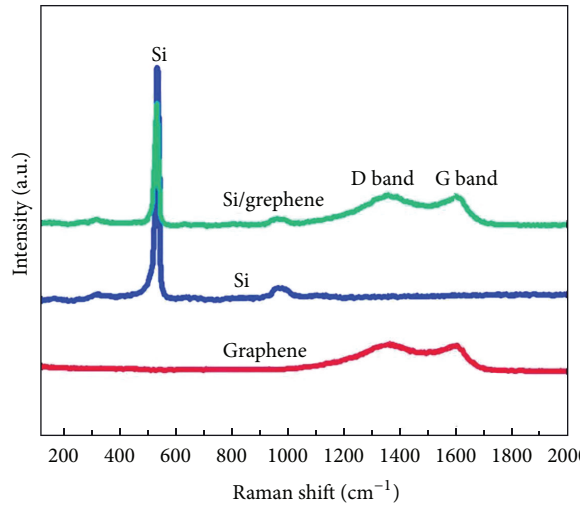

Figure 2: Raman spectra of the Si/graphene composites, Si nanoparticles, and graphene.

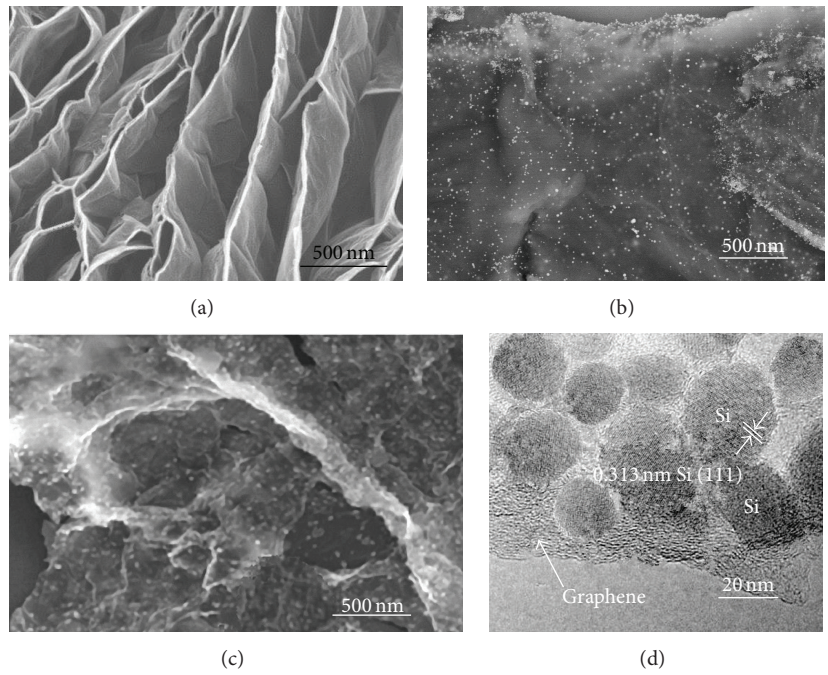

Figure 3: SEM images of (a) graphene, (b) Si nanoparticles/graphene composite, and (c) Si nanoparticles/graphene anode after 40 cycles between 0.02 and 1.5 V with 100 mAhg^{-1} charge/discharge current density and (d) TEM images of Si nanoparticles/graphene composite.

agreement with the data in the spectrum of Si nanoparticles, while the peaks at 1350 and 1596 cm^{-1} correspond to the D band and the G band, respectively, which are characteristic Raman peaks for carbon materials, indicating the presence of graphene. The intensity of the D band is comparable to that of the G band in the Si/graphene composites, which may be due to (1) a decrease in the average size of the new or more sp2 domains during the reduction and (2) the presence of a few defects or residual oxygen moieties that remain after the reduction of GO to graphene.

SEM and TEM images clearly display the composite morphology (Figure 3). The special wrapping structure of graphene benefited from the stacking and folding of graphene (Figure 3(a)). All Si nanoparticles have fine, uniform particle sizes ranging from 30 to 50 nm (Figures 3(b)–3(d)). The inner structure of the particles cannot be clearly observed due to the crinkled but close stacking of graphene (Figure 3(b)). From Figure 3(c), it can be seen that the nanostructure of Si/graphene composite is well retained even after intensive cycling. The original particle size of the Si/graphene composite is retained and no more agglomeration is detected. Moreover, it is clearly observed from Figure 3(d) that the wrapped Si nanoparticles are evenly dispersed in the composite particle. Si nanoparticles/graphene composite made the

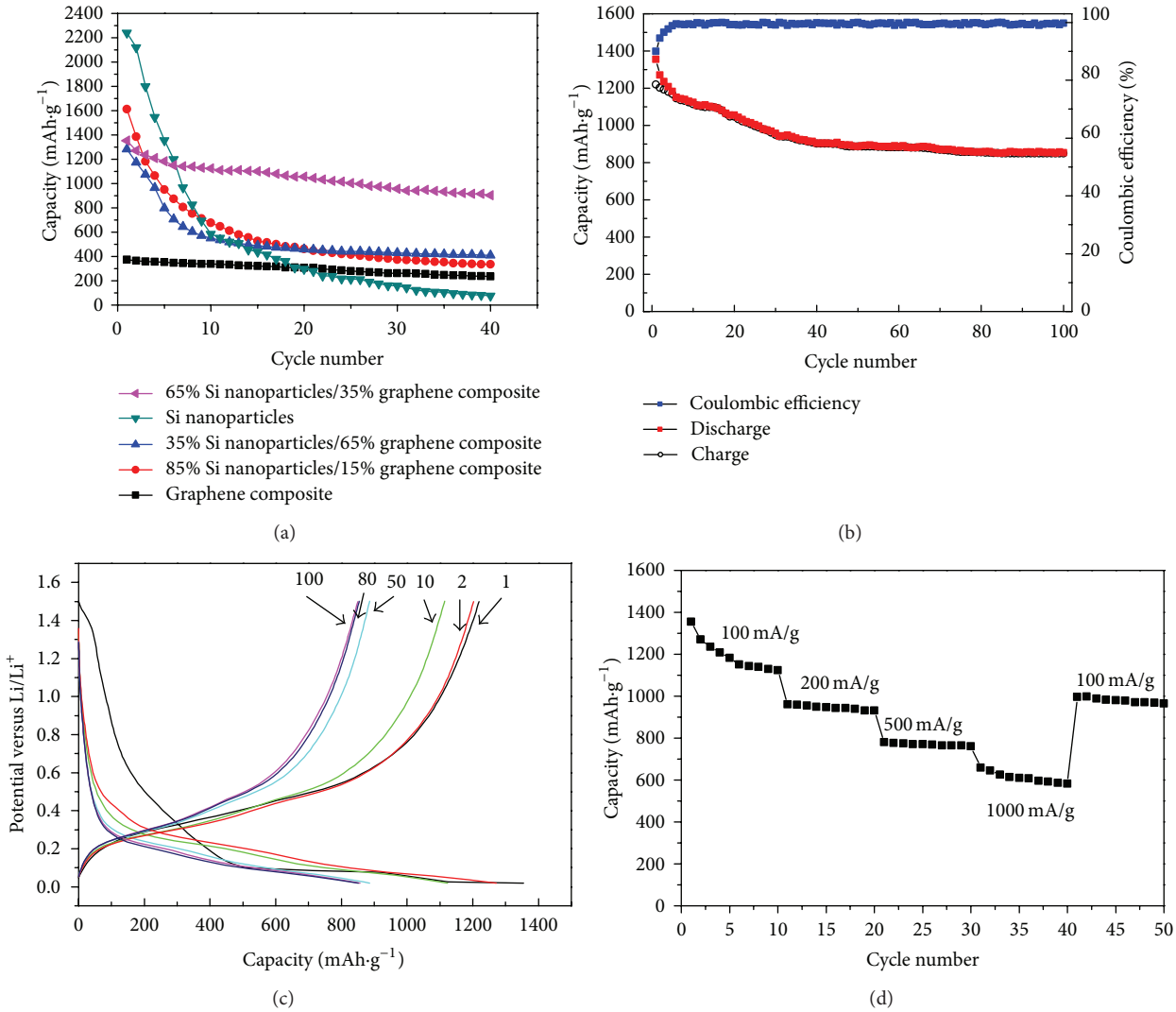

Figure 4: Electrochemical performance of the Si/graphene composites. (a) Cycling stability of the composites obtained in different Si nanoparticles and graphene weight ratios. (b) Long-term cycling stability of the Si/graphene composites under current density of 100 mAg^{-1}. (c) Charge/discharge profiles of the Si/graphene composites obtained after one, two, four, fifty, eighty, and one hundred cycles. (d) Rate performance of the Si/graphene composites.

materials form the bigger and denser sinters and was fit for lithium ion battery preparation.

3.2. Cycle Performance Studies. The cycle performances of anode of different Si nanoparticles and graphene ratios are displayed in Figure 4(a). Visibly, at a rate of 100 mAg^{-1}, all composites have better capacity retention than the Si nanoparticles or graphene, because of better dispersion of Si nanoparticles in the graphene sheet. The synthesis process leads the Si nanoparticles dispersing well on the graphenes, which guarantees that there is abundant interspace between the Si nanoparticles. The abundant interspace can accommodate the volume swing of Si nanoparticles in the charge/discharge processes effectively, which also keeps the Si-based anodes to maintain stable in cycling. The material of 65% Si nanoparticles exhibits the highest capacity after 40 cycles. The high reserve rate of sample 65% Si nanoparticles after 40 cycles is a significant improved property compared with other Si and graphene composite materials. Nevertheless, only the composite with weight ratios of 65 : 35 has the highest capacity after 40 cycles. This means that the cycle performances of the Si nanoparticles/graphene composite are visibly influenced by the concentration of the graphenes in the composite, which affects the Si nanoparticles dispersion severely. The materials exhibit a low capacity when there are more graphenes due to the lower content of Si nanoparticles. On the contrary, the materials have a larger initial capacity. But the capacity decreases gradually like the pristine Si nanoparticles, because there are no enough graphenes to construct the frame work, resulting in the Si nanoparticles aggregating. Thus, the material of 65% Si nanoparticles/35% graphene composite has the largest initial capacity.

Figure 4(b) indicates that the 65% Si nanoparticles/35% graphene composite shows good cycling performance, and the capacity retention after 20 cycles is 96.72%. The initial capacity of the sample 65% Si nanoparticles is 1354 mAg^{-1}, and this value falls to 1271 mAg^{-1} at the second cycle. Then, it keeps above 850 mAg^{-1} at the 100th cycle. This is because parts of the active materials are not completely utilized during the first cycles, and they are activated along with the charge/discharge process, which makes the diffusion path of Li^+ wider and results in the capacity enhancement of the material. The excellent cycle performances are caused by the good structure of the composites, which ensured uniform electronic conducting sheet and intensified the cohesion force of binder and collector, respectively.

Figure 4(c) shows the charge/discharge profiles of the composite under current density of 100 mAg^{-1} after one, two, ten, fifty, eighty, and one hundred cycles. A long discharge plateau below 0.3 V due to the Si crystalline structure was observed in the first discharge. The first discharge and charge capacities are 1354 and 1218 $mAhg^{-1}$, respectively, and the initial coulombic efficiency is 89.9%. The first cycle irreversible capacity loss mainly originated from the reduction of the electrolyte, resulting in the formation of the solid electrolyte interphase (SEI) film on the surface of the Si nanoparticles and the graphene, or from irreversible Li^+ insertion into the composite. After the first cycle, the crystalline structure nano-Si transforms to amorphous nano-Si, which can be proved from the shift of the subsequent discharge curves.

Figure 4(d) shows a rate capability of Si nanoparticles/graphene composite electrode indicating superior rate capability. At a rate of 100 mAg^{-1}, reversible capacity was about 1100 mAg^{-1}, and the reversible capacity at a rate of 1000 mAg^{-1} (approximately 3 C rate for the case of graphite electrode) was over 600 $mAhg^{-1}$. This excellent rate capability was caused by graphene sheets in which inner nanosize Si particles are under 100 nm. Although the movement of Li^+ through the inside of Si particle was sluggish in general, shorter diffusion path of Li^+ within the nanosize Si in this study was a significant advantage to get an excellent rate capability. Additionally, the advantage of the process employed in this study was very simple and possible to prepare a large amount of electrode materials at just one time compared to other processes.

3.3. Cyclic Voltammetry Studies. The CV curves of 65% Si nanoparticles/35% graphene composite electrode are shown in Figure 5. During the first half-cycle (Li-ion insertion), a peak observed at around 0.75 V could be attributed to the formation of SEI film. The peak disappears in the subsequent cycles. This phenomenon explains the low initial CE in the galvanostatic charge/discharge tests. One additional peak appears near 0.15 V in the subsequent cycles, which can be ascribed to the formation of Li-Si alloys. Two broad anodic peaks occur at around 0.37 V and 0.55 V corresponding to the phase transition between Li-Si alloys and Si. It is notable that the delithiation current peaks exhibit an enhanced intensity from the first cycle to the fifth cycle gradually, which can be attributed mainly to the gradual breakdown of the silicon structure that depends on the migration rate of Li-ions into the silicon and the rate of amorphous Li-Si alloy formation.

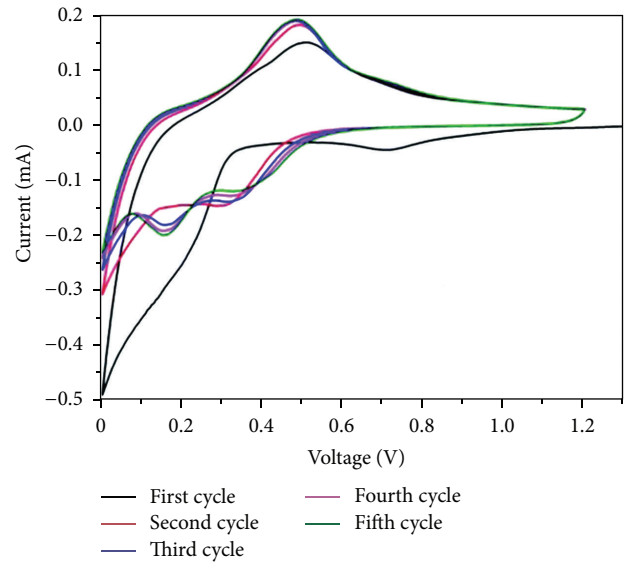

Figure 5: The CV curves of 65% Si nanoparticles/35% graphene composite, $\nu = 0.1$ mV/s.

4. Conclusion

In summary, we demonstrate a facile, low-cost, and scalable approach to prepare the Si/graphene composites for high performance LIBs. The approach has enabled preparation of a well-defined self-assembly structure of Si nanoparticles with spatially defined wrap of graphene. This unique structure enhances electron diffusion and conductivity of Si nanoparticles. More importantly, the self-assembly structure can accommodate Si expansion during lithiation and delithiation cycling, thus significantly improving the discharge capacity and prolonging the anode life in contrast to bare Si anodes materials. The prepared Si/graphene composite has a favorable structure for its application in LIBs. On one hand, the graphene enhances the electronic conductivity of Si nanoparticle and the void spaces between Si nanoparticles facilitate the lithium ion diffusion. On the other hand, the flexible graphene and the void spaces can effectively decrease the volume expansion of Si nanoparticles. The initial capacity of the Si/graphene keeps above 850 $mAhg^{-1}$ after 100 cycles at a rate of 100 mAg^{-1}.

Conflict of Interests

The authors declare that they have no conflict of interests regarding the publication of this paper.

References

[1] B. Scrosati and J. Garche, "Lithium batteries: status, prospects and future," *Journal of Power Sources*, vol. 195, no. 9, pp. 2419–2430, 2010.

[2] Y. Eker, K. Kierzek, E. Raymundo-Piñero, J. Machnikowski, and F. Béguin, "Effect of electrochemical conditions on the performance worsening of Si/C composite anodes for lithium batteries," *Electrochimica Acta*, vol. 55, no. 3, pp. 729–736, 2010.

[3] X. Wang, Z. Wen, Y. Liu, X. Xu, and J. Lin, "Preparation and characterization of a new nanosized silicon-nickel-graphite composite as anode material for lithium ion batteries," *Journal of Power Sources*, vol. 189, no. 1, pp. 121–126, 2009.

[4] C. Liu, F. Li, L.-P. Ma, and H.-M. Cheng, "Advanced materials for energy storage," *Advanced Materials*, vol. 22, no. 8, pp. E28–E62, 2010.

[5] S. Pan, "Manufacture method of environment-friendly high-capacity lithium ion battery," p. 7, China, 2010.

[6] Y.-S. Wu, Y.-H. Lee, and Y.-L. Tsai, "The improvement on capacity retention of silicon/graphite composites with TiN additive as anode materials for Li-ion battery," *Journal of Materials Processing Technology*, vol. 208, no. 1–3, pp. 35–41, 2008.

[7] A. M. Chockla, K. C. Klavetter, C. B. Mullins, and B. A. Korgel, "Tin-seeded silicon nanowires for high capacity li-ion batteries," *Chemistry of Materials*, vol. 24, no. 19, pp. 3738–3745, 2012.

[8] K. E. Aifantis, S. Brutti, S. A. Hackney, T. Sarakonsri, and B. Scrosati, "SnO_2/C nanocomposites as anodes in secondary Li-ion batteries," *Electrochimica Acta*, vol. 55, no. 18, pp. 5071–5076, 2010.

[9] J. Yu, N. Du, J. Wang, H. Zhang, and D. Yang, "SiGe porous nanorod arrays as high-performance anode materials for lithium-ion batteries," *Journal of Alloys and Compounds*, vol. 577, pp. 564–568, 2013.

[10] H.-K. Seong, M.-H. Kim, H.-J. Choi, Y.-J. Choi, and J.-G. Park, "Electrochemical characteristics of single crystalline nanowires and their driven mechanism," *Metals and Materials International*, vol. 14, no. 4, pp. 477–480, 2008.

[11] Y. Liu, Z. Y. Wen, X. Y. Wang et al., "Improvement of cycling stability of Si anode by mechanochemcial reduction and carbon coating," *Journal of Power Sources*, vol. 189, no. 1, pp. 480–484, 2009.

[12] V. P. Phan, B. Pecquenard, and F. Le Cras, "High-performance all-solid-state cells fabricated with silicon electrodes," *Advanced Functional Materials*, vol. 22, no. 12, pp. 2580–2584, 2012.

[13] Y. Nagaura, K. Imani, and K. Seike, "The secondary battery module of a silica electrode, and a method for manufacturing [Machine Translation]," p. 33, Japan, 2013.

[14] L. Zhang, F. Wang, P. Liang et al., "The electrochemical properties of melt-spun Al-Si-Cu alloys," *Materials Chemistry and Physics*, vol. 129, no. 3, pp. 1006–1010, 2011.

[15] F. Thoss, L. Giebeler, S. Oswald, H. Ehrenberg, and J. Eckert, "Study on the reversible Li-insertion of amorphous and partially crystalline $Al_{86}Ni_8La_6$ and $Al_{86}Ni_8Y_6$ alloys as anode materials for Li-ion batteries," *Electrochimica Acta*, vol. 60, pp. 85–94, 2012.

[16] J. Rohrer and K. Albe, "Insights into degradation of Si anodes from first-principle calculations," *The Journal of Physical Chemistry C*, vol. 117, no. 37, pp. 18796–18803, 2013.

[17] L.-F. Cui, L. Hu, J. W. Choi, and Y. Cui, "Light-weight free-standing carbon nanotube-silicon films for anodes of lithium ion batteries," *ACS Nano*, vol. 4, no. 7, pp. 3671–3678, 2010.

[18] J. L. Gómez Cámer, J. Morales, L. Sánchez et al., "Nanosized Si/cellulose fiber/carbon composites as high capacity anodes for lithium-ion batteries: a galvanostatic and dilatometric study," *Electrochimica Acta*, vol. 54, no. 26, pp. 6713–6717, 2009.

[19] Y. Chao, X. Yuan, and Z. Ma, "Preparation and characterization of carbon cryogel (CC) and CC-SiO composite as anode material for lithium-ion battery," *Electrochimica Acta*, vol. 53, no. 9, pp. 3468–3473, 2008.

[20] I. A. Profatilova, N.-S. Choi, K. H. Yew, and W. Choi, "The effect of ethylene carbonate on the cycling performance of a Si electrode," *Solid State Ionics*, vol. 179, no. 40, pp. 2399–2405, 2008.

[21] J. M. Yan, H. Z. Huang, J. Zhang, and Y. Yang, "The study of Mg_2Si/carbon composites as anode materials for lithium ion batteries," *Journal of Power Sources*, vol. 175, no. 1, pp. 547–552, 2008.

[22] S. Rousselot, M. Gauthier, D. Mazouzi, B. Lestriez, D. Guyomard, and L. Roué, "Synthesis of boron-doped Si particles by ball milling and application in Li-ion batteries," *Journal of Power Sources*, vol. 202, pp. 262–268, 2012.

[23] Q. Si, K. Hanai, T. Ichikawa et al., "Improvement of cyclic behavior of a ball-milled SiO and carbon nanofiber composite anode for lithium-ion batteries," *Journal of Power Sources*, vol. 196, no. 22, pp. 9774–9779, 2011.

[24] F. Sauvage, L. Laffont, J.-M. Tarascon, and E. Baudrin, "Factors affecting the electrochemical reactivity vs. lithium of carbon-free $LiFePO_4$ thin films," *Journal of Power Sources*, vol. 175, no. 1, pp. 495–501, 2008.